

# Competitive Mechanism of Stereocomplexes and Homocrystals in High-Performance Symmetric and Asymmetric Poly(lactic acid) Enantiomers: Qualitative Methods

Mingwei Guo, Wenjing Wu, Weixin Wu, and Qinwei Gao\*

Cite This: *ACS Omega* 2022, 7, 41412–41425

Read Online

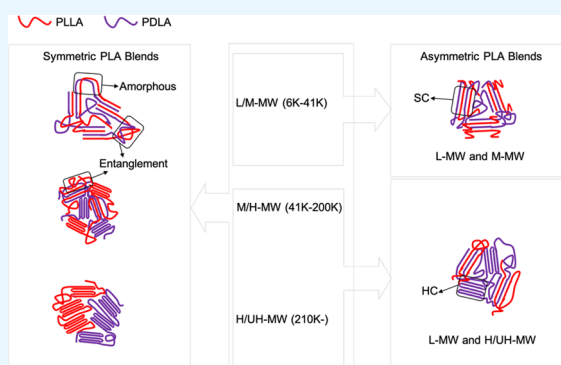
ACCESS |

Metrics &amp; More

Article Recommendations

Supporting Information

**ABSTRACT:** To systematically explore the critical contributions of both molecular weights and crystallization temperature and chain length and molar ratios to the formation of stereocomplexes (SCs), our group quantitatively prepared a wide MW range of symmetric and asymmetric poly(lactic acid) (PLA) racemic blends, which contains L-MW PLLA with  $M_n > 6k$  g/mol. The crystallinity and relative fraction of SCs increase with  $T_c$  and the SCs are exclusively formed at  $T_c > 180$  °C in M/H-MW racemic blends. When MWs of one of the enantiomers are over 6k and less than 41k, multiple stereocomplexation is clear in the asymmetric racemic blends and more ordered SCs form with less entanglement or the amorphous region compared to those for the MW of the enantiomers over 41k in the symmetric/asymmetric enantiomers. When the MW of the blends is more than 41k, SCs and homocrystals (HCs) coexist in the symmetric enantiomers and the multicomplexation can restrict the asymmetric enantiomers. This study provides a deep comprehensive insight into the stereocomplex crystallization mechanism of polymers and provides a reference value for future research attempting to prepare stereocomplex materials.



## 1. INTRODUCTION

Poly(lactic acid) (PLA) has been widely used in biomedical and commercial applications to replace conventional oil-based thermoplastics.<sup>1–5</sup> The melting temperature of conventional PLA, i.e., poly(L-lactide) (PLLA), is around 170 °C and its glass transition temperature ( $T_g$ ) is about 60 °C. However, homocrystalline PLA suffers from disadvantages, such as low end-use temperature and low hydrolytic durability.<sup>6</sup> Its thermal resistance is limited by a relatively low heat deflection temperature due to the slow crystallization and low crystallizability in practical processing such as injection molding.<sup>2,3</sup> It is worth mentioning that the presence of chiral carbon in the skeletal chain of PLA results in two stereoregular enantiomers, namely poly(L-lactide) (PLLA) and poly(D-lactide) (PDLA). The PLLA/PDLA racemic blends lead to the formation of SCs with denser chain packing and stronger interchain interactions.<sup>7–10</sup> The chemical and physical properties of the stereocomplex poly(lactic acid) (sc-PLA) strongly exceed those of its parent enantiomeric pure, homocrystalline polymers, such as higher mechanical strength, better thermal stability, lower thermodegradation, etc.<sup>11–13</sup> Meanwhile, this specific complex structure can effectively solve the above-mentioned limitations. Since this first report, the influences of the homopolymer molecular weight, blending ratio, blending conditions, and optical purity on the formation and properties of stereocomplexes have been well investigated.<sup>14–21</sup>

However, not all of the medium/high-molecular weight (M/H-WM) PLLA/PDLA blends can achieve perfect stereocomplexation, i.e., without any homocrystallization of PLLA or PDLA. Pan et al.<sup>21</sup> found that the MW is a crucial factor influencing the competition of HCs and SCs and crystalline transition of PLLA/PDLA racemic blends. It has been well demonstrated that in the 1:1 asymmetric M/H-MW of PLLA/PDLA blends, SC formation is preferential, and apart from this composition, homocrystals from either PLLA or PDLA are induced. The molecular weights of PLLA and PDLA have profound influences on the competing formation of SCs and HCs in their enantiomeric blends. There exists a critical molecular weight of about  $10^5$  g/mol, beyond which it is difficult to form stereocomplexations.<sup>22</sup> Because both enantiomers of PLLA and PDLA must combine in stereocomplexation, they have a larger diffusion path than that of regular homocrystallization. The critical molecular weights for PLLA and PDLA to achieve exclusive/unique stereocomplexation in melt crystallization and solution crystallization have been found to be about

Received: August 13, 2022

Accepted: October 21, 2022

Published: November 7, 2022



6k and 40k g/mol, respectively.<sup>23,24</sup> When the MW is less than 40k g/mol, furthermore, the MWs and composition (i.e., the ratio between PLLA and PDLA) are the two direct and critical factors that determine the formation of SCs in the asymmetric PLLA/PDLA.<sup>25–28</sup> Dong et al.<sup>29</sup> investigated the contribution of chain length and mole ratios via a specially prepared library of the discrete *o*LA with MW < 4k g/mol. Interestingly, this *o*LA not only effectively avoided the issues of amorphous-state formation due to entanglement but also formed an expanded chain conformation to conveniently explore the contribution of the chain length and molar ratios to the formation of SCs. From a practical view, however, a high molecular weight is a precondition for obtaining excellent mechanical performances of polylactides.<sup>22</sup> Therefore, in the past, extensive efforts have been devoted to achieving high stereocomplexation from polylactides with H-MW by various preparation methods, for instance, repeat casting, supercritical fluid technology, low-temperature blending, and so on.<sup>30</sup> Tashiro et al.<sup>31,32</sup> found that SCs can be formed in the PLLA/PDLA ratio from 70/30 to 30/70 and provide a possibility for multicomplexation in the M/H-MW PLLA/PDLA racemic blends.

Due to the difficulty of determination of stoichiometry in crystalline and amorphous regions of sc-PLA, in which HCs and the amorphous state are difficult to be assigned explicitly to one of the enantiomers,<sup>7</sup> there are still few research groups and co-workers studying the effects of the MW and molar ratios on the formation of SCs and HCs for PLLA/PDLA racemic blends with  $M_n > 6k$  g/mol. It is well known that stereocomplexation is favorable for the PLLA/PDLA blend, which contains at least one low-MW (L-MW) enantiomer. To systematically explore the critical contributions of both molecular weights and crystallization temperature and chain length and molar ratios to the formation of SCs, our group attempted to quantitatively prepare a wide MW range of symmetric and asymmetric PLA racemic blends, which contains L-MW PLLA with  $M_n > 6k$  g/mol. More importantly, the investigation of multicomplexation through asymmetric PLA racemic blends can provide an idea to address the limitations of H-WM PLLA/PDLA racemic blends.

## 2. EXPERIMENTAL SECTION

**2.1. Materials.** Both L- and D-lactic acid (optical purities >99.5%) were purchased from Musashino Chemical Co., Ltd. (Yichun, China). Tin(II) 2-ethylhexanoate [Sn(Oct)<sub>2</sub>, >99.9%] was purchased from Shanghai Jiuyi Chemical Reagent Co., Ltd., China. All these materials were used without purification. PLLA and PDLA with various L/M-MWs were synthesized by melt/solid polymerization using Sn(Oct)<sub>2</sub> as the catalyst. The detailed synthesis steps are shown in Figure S1 (Supporting Information). The PLLA and PDLA with H-MWs were synthesized by bulk ring-opening polymerization at 130 °C using diacetone-D-glucose and lauryl alcohol as the initiator and Sn(Oct)<sub>2</sub> as the catalyst. The samples were purified by precipitation into methanol from the chloroform solution and then were dried under vacuum at 50 °C for 24 h. The MWs and polydispersity index (PDI) of PLLA and PDLA are listed in Table S1.

**2.2. Preparation of Various Mixing Ratios of Symmetric and Asymmetric Polylactide Enantiomers.** PLLA and PDLA were dissolved in chloroform separately and were solution-blended at different PLLA/PDLA ratios, coded as L<sub>x</sub>/D<sub>y</sub> and L<sub>m</sub>/D<sub>n</sub> ( $n_L/n_D$ ), where  $n_L/n_D$  represents their mole ratio according to the weight-averaged molecular weights, in which L and D represent PLLA and PDLA, respectively;  $x$  and  $y$

represent the weight-averaged molecular weights ( $M_w$ , kg/mol) of PLLA and PDLA, respectively; and  $m$  and  $n$  represent the average degree of the L/M-MW PLLA and PDLA, which refers to the number of repeat units according to NMR, respectively. The samples are not indicated whose mole ratio is 1:1 based on  $M_w$  for all samples. The prepared solutions are mixed together with vigorous stirring for 10 min; then, the racemic mixture was poured in the mold of polytetrafluoroethylene to naturally volatilize chloroform. All samples were followed by drying under vacuum at 60 °C for 10 h, after erasing the thermal history and being subsequently crystallized at temperature  $T_c = 80–200$  °C.

## 3. CHARACTERIZATIONS

**3.1. Differential Scanning Calorimetry (DSC).** DSC measurements were performed on a NETZSCH DSC-200F3 differential scanning calorimetry instrument (NETZSCH-Gerätebau GmbH, Selb, Germany) equipped with an IC70 intracooler. The sample sealed in an aluminum pan was first heated to 250 °C and held for 5 min to eliminate the thermal history. To investigate the melting behavior, the sample was cooled from 250 to 20 °C and then reheated to 250 °C again under a nitrogen gas flow of 60 mL/min. Both the heating rate and cooling rate were 10 °C/min. The temperature and enthalpy of melt crystallization upon cooling ( $T_{mc}$ ,  $\Delta H_{mc}$ ), the temperature and enthalpy of cold crystallization upon subsequent second heating ( $T_{cc}$ ,  $\Delta H_{cc}$ ), and the melting temperature and enthalpy of HCs ( $T_{m,hc}$ ,  $\Delta H_{m,hc}$ ) and SCs ( $T_{m,sc}$ ,  $\Delta H_{m,sc}$ ) were calculated on the basis of the DSC curves. For investigating isothermal melt crystallization, the samples were rapidly cooled from 250 °C to the desired temperature at a rate of 100 °C/min and then kept at this temperature for crystallization. It was then reheated to 250 °C to examine the melting behavior.<sup>21</sup>  $\Delta H_{m,hc}$  and  $\Delta H_{m,sc}$  were evaluated from the DSC melting curves. Degrees of crystallinity for HCs ( $X_{hc}$ ) and SCs ( $X_{sc}$ ) were estimated by comparing  $\Delta H_m$  to the corresponding value of an infinitely large crystal ( $\Delta H_m^0$ ), which were  $\Delta H_m^0 = 93.6$  and 142 J/g for HCs and SCs,<sup>33,34</sup> respectively. The relative fraction of SCs in the crystalline phase of PLLA/PDLA racemic blends was calculated by  $f_{SC,DSC} = X_{sc}/(X_{sc} + X_{hc})$ .

**3.2. X-ray Diffraction (XRD).** XRD analysis of melt-crystallized PLLA/PDLA blends was performed on a Rigaku XRD Ultima IV instrument (Rigaku Corporation, Tokyo, Japan) with a D/teX-Ultra using Ni-filtered Cu K $\alpha$  radiation ( $\lambda = 0.154$  nm), operated at 40 kV and 30 mA. The sample was step-scanned from 5 to 40° at a  $2\theta$  scanning rate of 5°/min. The sample was prepared by the same thermal procedure as that used in DSC. On the basis of XRD results, the relative fraction of SCs ( $f_{sc,XRD}$ ) in the crystalline phase of the PLLA/PDLA mixture was estimated by comparing the diffraction peak area of SCs with the total peak areas of both SC and HC diffractions, that is,  $f_{sc,XRD} = I_{sc}/(I_{sc} + I_{hc})$ , in which  $I_{sc}$  and  $I_{hc}$  are the peak areas of SC and HC diffractions, respectively.

**3.3. Polarized Optical Microscopy (POM).** Polarizing optical microscopy (POM) images were acquired under nitrogen atmosphere protection using a polarizing microscope instrument (Eclipse E200 POL, Nikon, Japan) equipped with a hot stage (LTS420, Linkam Scientific Instruments). This setup was used to track the nucleation and spherulitic growth for the PLLA/PDLA racemic blends during isothermal crystallization. The PLLA/PDLA racemic blends were melted at 240 °C for 5 min to remove the thermal history and then were quickly cooled to 120 °C at a cooling rate of 50 °C/min. Once the sample temperature reached 120 °C, the polarized optical micrographs

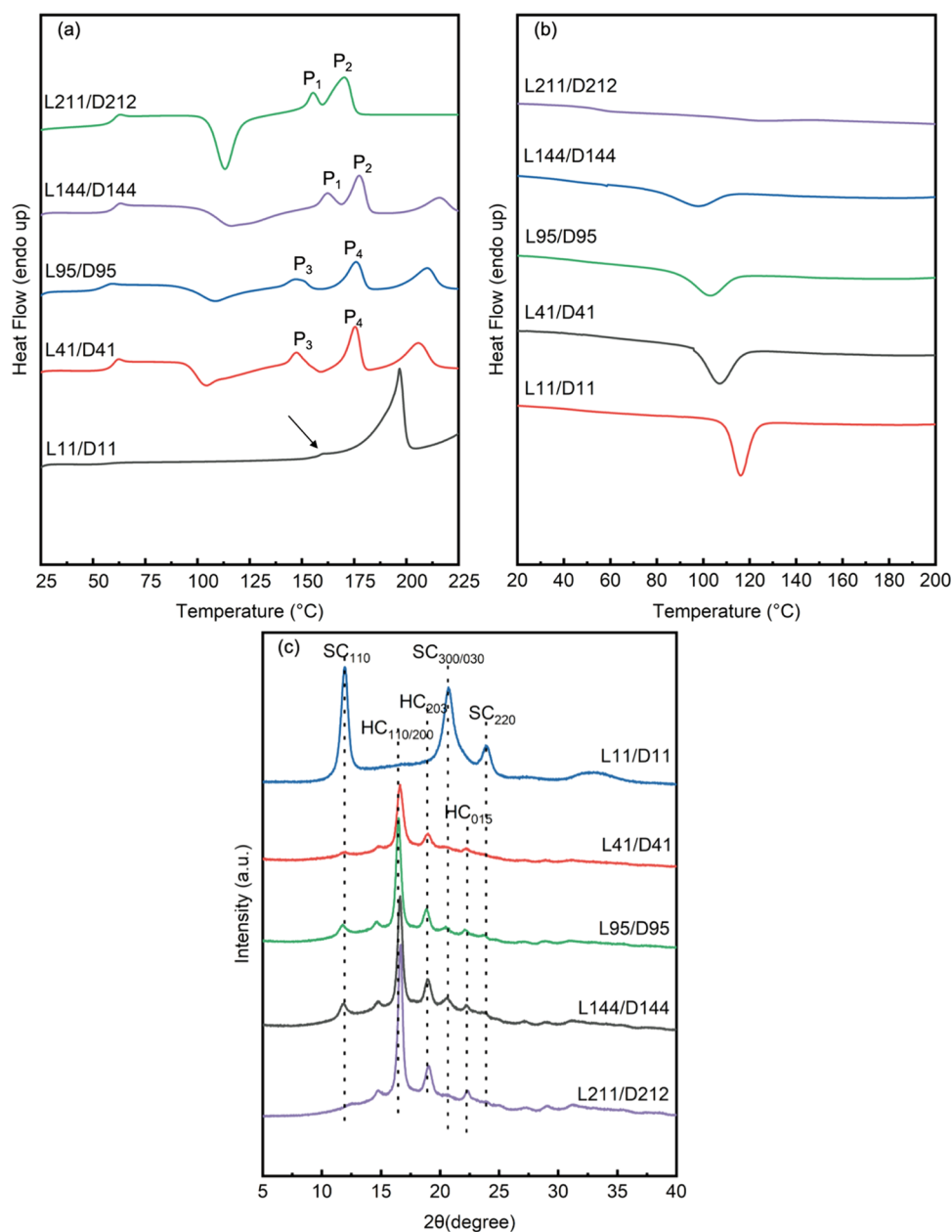


**Figure 1.** DSC melting curves of the symmetric PLLA/PDLA racemic blends collected upon the second subsequent heating (a) and first cooling (b); XRD patterns (c) of the symmetric PLLA/PDLA blends.

**Table 1. Thermal Parameters of Symmetric PLLA/PDLA Racemic Blends Collected upon Nonisothermal Melt Crystallization and Subsequent Melting**

sample	cooling		subsequent heating						$f_{sc,XRD}$ (%)
	$T_{mc}$ (°C)	$\Delta H_{mc}$ (J/g)	$T_{cc}$ (°C)	$\Delta H_{cc}$ (J/g)	$T_{m,hc}$ (°C)	$\Delta H_{m,hc}$ (J/g)	$T_{m,sc}$ (°C)	$\Delta H_{m,sc}$ (J/g)	
L11/D11	116.5	-38.44		0		0	196.5	37.94	100
L41/D41	107.2	-37.05	104.9	-14.17	147.6, 175.6	7.98, 15.78	206.1	14.58	10
L95/D95	103.3	-12.87	108.4	-17.81	148.7, 176.3	5.71, 12.09	211.0	13.07	8
L144/D144	98.2	-3.32	115.5	-20.43	162.2, 177.9	3.81, 12.20	215.8	7.03	5
L211/D212	89.4	-0.53	116.7	-25.66	159.6, 165.5	3.34, 14.99		0	0

were taken at appropriate time intervals.<sup>20</sup> The changes in nucleation density and spherulitic growth of the samples were traced until the impingements of the growing spherulites occurred. All samples were dried at 50 °C for 10h before detection.

## 4. RESULTS AND DISCUSSION

### 4.1. Crystallization Kinetics and Crystal Morphology of the Symmetric PLLA/PDLA Racemic Blends.

The crystallization kinetics and melting behavior of symmetric PLLA/PDLA racemic blends with different MWs were first

investigated by the DSC curves. Figure 1 shows the DSC thermograms recorded upon subsequent heating and cooling. The thermal parameters that were derived from the DSC curves are shown in Table 1. As shown in Figure 1, the crystallization kinetics and melting behavior of symmetric PLLA/PDLA racemic blends depended strongly on the molecular weight. Upon heating, both  $T_{cc}$  and  $\Delta H_{cc}$  increased with increasing molecular weight (Table 1). When the heating rate was fixed (10 °C/min), the PLLA/PDLA of L-MW blends had short-molecular length chains, in which the mutual entanglement was weak, and it was easy to adjust the conformation for orderly stacking crystallization, which shows the lower cold crystallization temperature ( $T_{cc}$ ) than that of the M/H-MW symmetric racemic blends. As seen in Figure 1a, the L-MW racemic blends (e.g., L11/D11) show a melting region at a high temperature of ~200 °C, corresponding to the melting peak of SCs. However, the M/H-MW symmetric PLLA/PDLA racemic blends (e.g., L41/D41, L95/D95, L144/D144) exhibit two melting regions at 140–180 and ~210 °C upon heating. The melting endotherms at low (~140 and ~180 °C) and high (~210 °C) temperatures corresponded to HCs and SCs, respectively. These results demonstrated that the SCs were exclusively formed in L-MW racemic blends, whereas the mixture of HCs and SCs was generated in the M/H-MW racemic blends. Notably,  $\Delta H_{m,sc}$  decreased steadily, while  $\Delta H_{m,hc}$  first increased and then decreased, as the MWs of PLLA and PDLA increased (Table 1). Thus, it can be concluded that the formation of the stereocomplex of PLLA and PDLA was favorable in L-MW racemic blends but drastically suppressed in the M/H-MW racemic blend. The inhibition of stereocomplexation in M/H-MW racemic blends was assumed to be due to the low chain diffusion ability and restricted intermolecular crystal nucleation/growth. Figure 1a also shows that the UH-MW PLLA/PDLA blends (e.g., L211/D212) can hardly/not form stereocomplexation. Due to the extremely high degree of entanglement and low chain diffusion ability, the UH-MW PLLA/PDLA blends hardly formed SCs by solution mixing for a short time. This was consistent with the existing experimental results.<sup>20,21,35,36</sup> These results suggested that chain entanglements played a crucial role in SC crystallization compared with common homocrystallization. This conclusion was supported by the strong MW dependence of SC crystallization since the major difference between L- and H-MW polymers was the degree of entanglement.

Meanwhile, it is notable that the extensive molecular weight range of symmetric PLLA/PDLA racemic blends (e.g., L41/D41, L95/D95, etc.) shows multiple melting peaks upon heating. For L41/D41 and L95/D95, the endotherm peak  $P_3$  at ~150 °C and the peak  $P_4$  at ~175 °C can belong to the  $\alpha'$ -form and the  $\alpha$ -form of PLLA, respectively. This is because when samples are dried at 60 °C for a long time, parts of the amorphous state form a small amount of the  $\alpha'$ -form under a low-crystallization temperature atmosphere.<sup>37</sup> The amorphous state due to the large amount of entanglement is difficult to transform directly into the  $\alpha'$ -form PLLA in the H/UH-MW racemic blends. For L144/D144 and L211/D212, however, the endotherm peak  $P_3$  and the peak  $P_4$  appear upon second heating, which may be attributed to the melt recrystallization mechanism. The endotherm  $P_1$  can be attributed to the melting of preliminary crystals developed in nonisothermal crystallization, and the peak  $P_2$  is ascribed to the melting of crystallites formed in recrystallization upon heating. This is ascribed to the formation of more perfect crystallites with high melting

temperatures. Thus, the low- and high-temperature side endotherms are derived from the melting of the original homocrystals and those reorganized homocrystals during the DSC heating scan, respectively.<sup>38</sup> Moreover, it is noticed that a shoulder appears at the right side of  $T_{m,sc}$  of L11/D11 (pointed out by a black arrow) in Figure 1a, located at 151.6 °C. Note that  $T_{m,hc}$  for neat PLLA<sub>30</sub> is 150.1 °C (Figure S5). The shoulder is apparently due to the melting of PLLA crystals of a minor quantity in L11/D11 blends.

As seen in Figure 1b, when the MWs of PLLA and PDLA is less than ~41k, the racemic blend exhibits quick crystallization, and it can complete crystallization upon cooling at 10 °C/min. However, when the MWs of PLLA and PDLA increased above 41k, a cold crystallization peak ( $T_{cc}$ ) is detected in the subsequent heating. Upon cooling, both  $T_{mc}$  and  $\Delta H_{mc}$  decrease with increasing MW, as shown in Table 1. These results suggest that the crystallization rate of the symmetric PLLA/PDLA racemic blends decreases with increasing MW, similar to the molecular weight-dependent crystallization kinetics of pure PLA.<sup>39</sup> When the cooling rate is fixed (10 °C/min), the larger the molecular weight of PLA, the longer the molecular chain length of PLA, the lower the chain flexibility, and the more pronounced the entanglement with the molecular chain, which imply that the degree of the polymer molecular chain was lower during the adjustment, which is manifested a lower melting crystallization temperature ( $T_{mc}$ ). It is also notable that the synthesized PLLA and PDLA bear relatively long alkyl ends. Tsuji et al. have reported that the existence of long alkyl terminals in L-MW PLLA or PDLA (typically MW < 10 kg/mol) will increase the rates of homocrystal and stereocomplex crystallizations.<sup>40</sup> Due to the fact that L/M-MW of PLA is synthesized by melt/solid polymerization and the other PLA used here has relatively high MWs and all carry the same initiator terminal, the effect of the lauryl terminal on homocrystal and stereocomplex crystallization of symmetric PLLA/PDLA blends can be negligible.<sup>21</sup>

The isothermal crystallization and melting behavior of the PLLA/PDLA mixture with various MWs were further studied. To obtain the kinetic parameters, DSC curves collected in isothermal crystallization were analyzed by the Avrami equation. The Avrami equation is frequently employed to analyze the isothermal crystallization kinetics of polymers, according to which the relative degree of crystallinity  $X_t$ -dependent crystallization time  $t$  can be expressed as<sup>41–43</sup>

$$1 - X_t = \exp(-kt^n) \quad (1)$$

where  $X_t$  is the relative crystallinity,  $n$  is the Avrami exponent whose value usually depends on the dimension of crystal growth,  $t$  is the crystallization time, and  $k$  is the overall rate constant associated with both nucleation and growth contributions. The linear form of eq 1 can be expressed as follows

$$\log[-\ln(1 - X_t)] = \log k + n \log t \quad (2)$$

The Avrami parameters  $n$  and  $k$  can be obtained from the slopes and the intercepts, respectively.

$$\text{when } 1 - X_t = 1/2$$

$$t_{1/2} = (\ln 2/k)^{1/n} \quad (3)$$

In the case of the DSC experiment,  $X_t$  at  $t$  is defined as the ratio of the area under the exothermic curve between the onset crystallization time and  $t$  to the whole area under the exothermic curve from the onset crystallization time to the end

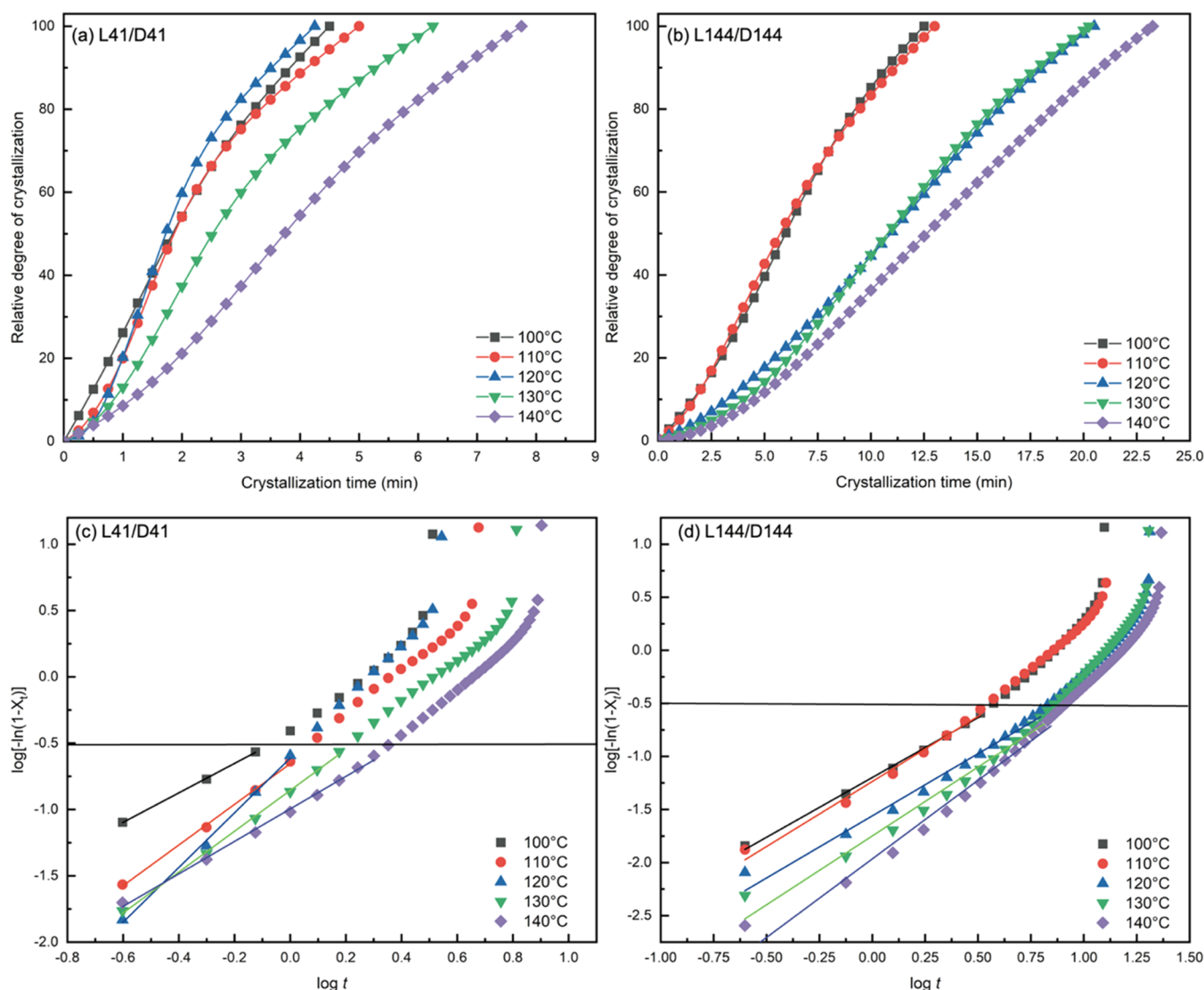


**Figure 2.** Variation of the relative degree of crystallinity with crystallization time at different  $T_c$  values for (a) L41/D41 and (b) L144/D144 and the related Avrami plots with  $X_t < 20\%$  for (c) L41/D41 and (d) L144/D144.

crystallization time (Figures 2a,b and S2a,b). Accordingly, the Avrami exponent  $n$  can be obtained from the slope in a plot of  $\log[-\ln(1 - X_t)]$  versus  $\log t$  (eq 2), as shown in Figures 2c,d and S2c,d. The crystallization half-time ( $t_{1/2}$ ) was obtained from the Avrami analysis (eq 3).

The Avrami parameters are summarized in the Supporting Information, Table S2, for PLLA/PDLA racemic blends crystallized at different  $T_c$  values. The values for  $n$  depend on the crystallization mechanism, and  $n$  usually is in the integer range from 1 to 4. It is found for various polymers that the  $n$  value adopts fractional numbers due to secondary crystallization. The values of  $n$  are found between 1.0 and 2.1, depending on the temperature and stereocomplexation content. A lower  $n$  value suggests that crystal growth may proceed in one dimension for  $X_t$  below 20%. The  $n$  value is smaller, possibly due to the faster crystallization mechanism that does not provide enough time to grow in three dimensions.<sup>44</sup>

Because the crystallization of L11/D11 ( $L_{30}/D_{30}$ ) blends was very fast at low  $T_c$ , their kinetics were analyzed by POM in the next section (Figure S9d).  $k$  and  $t_{1/2}$  of PLLA/PDLA racemic blends with different MWs are plotted as a function of  $T_c$  in

panels a and b of Figure 3, respectively. As shown in this figure (L41/D41, L95/D95, and L144/D144),  $t_{1/2}$  shows a minimum and  $k$  shows a maximum at around  $T_c = 110^\circ\text{C}$ , meaning that the racemic blends crystallize fastest around this  $T_c$ . The crystallization rate of racemic blends decreases as  $T_c$  is approaching  $T_g$  or  $T_m$ . The crystallization rate can be easily described as the reciprocal of  $t_{1/2}$  (Figure S3b). At the same  $T_c$ ,  $t_{1/2}$  increases, and  $k$  decreases with increasing MW, meaning the decrease of the crystallization rate. Due to investigation of the  $T_c$  range where only SCs are formed,  $T_c$  below  $115^\circ\text{C}$  was used to facilitate the investigation of isothermal crystallization effects for L211/D212. Although L211/D212 does not form stereocomplexes, we clearly found that the crystallization rate in relation to the crystallization temperature also follows this rule. In addition, the crystallization rate is much lower than that of sc-PLA.

**4.2. Melting Behavior and Multiple Crystalline Structure with Different Crystallization Temperatures.** Since SCs and HCs have distinct melting temperatures, the polymorphic structure of the PLLA/PDLA racemic blends crystallized at different  $T_c$  values can be evaluated by the melting

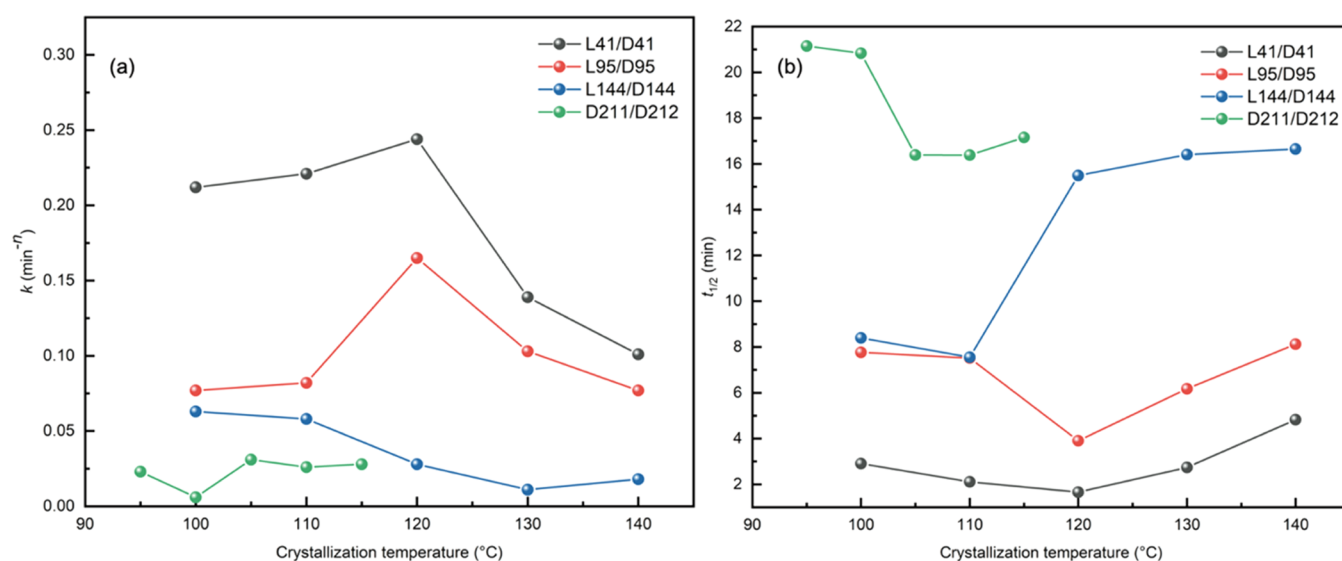


**Figure 3.** Plots of (a) overall crystallization rate constant and (b) crystallization half-time as a function of crystallization temperature for PLLA/PDLA racemic blends with different MWs.

behavior. The DSC melting curves of the PLLA/PDLA racemic blends crystallized by melting at different  $T_c$  values are shown in Figure 4. As shown in this figure, the melting behavior of the PLLA/PDLA racemic blends depends strongly on MW and  $T_c$ .

The L-MW racemic blend (e.g., L11/D11) merely shows a melting region at high  $T_c$  (200–210 °C) under all  $T_c$  values investigated, indicating the exclusive formation of SCs. This is consistent with the DSC data (Figure 4a), where only a melting peak of stereocomplexation is observed at  $\sim 200$  °C. It is worth mentioning that the melting temperature of SCs decreases with the increased crystallization temperature for L11/D11; the change is apparently due to the thermal degradation of SCs of a minor quantity in L-MW racemic blends. Hence, the multiple crystalline structures are not obviously caused by crystallization temperature in the L-MW blends. More perfect crystallites in which irregular stereocomplexes to regular stereocomplexes transition of the L-MW racemic blends takes place with increased melting temperature are formed in symmetric  $L_{52}/D_{52}$  blends (Figure S4). This is explained as more regular SCs formed via the recrystallization process from the disordered amorphous state in PLLA/PDLA racemic blends.<sup>21</sup>

For the M/H-MW racemic blends (L41/D41, L95/D95, and L144/D144), two melting regions corresponding to HCs of PLLA or PDLA and SCs of sc-PLA are observed at  $T_c < 140$  °C, indicating the formation of mixed HCs and SCs. A similar phenomenon (Figure 1a) which also shows multiple melting peaks ( $P_1, P_2$ ) is observed for M/H-MW blends crystallized at  $T_c = 120$  °C (Figure 4b,c). With further increasing  $T_c > 140$  °C, the double melting peaks ( $P_1, P_2$ ) amalgamated into one peak because the crystallites formed at high  $T_c$  are sufficiently perfect and do not undergo recrystallization upon heating. Because of the high melting point of the SC, it has a wider crystallization temperature region than that of HCs. When  $T_c$  is increased to a higher value than the melting point of homocrystallites (180–200 °C), SCs are exclusively formed in the M/H-MW racemic blends, showing the melting peak of SCs at high temperature (Figure 4b–d). The melting behavior and crystalline structure of homocrystallites in the M-MW and H-MW racemic blends also show  $T_c$  dependence. The multiple melting behavior of

homocrystallites has been ascribed to the phase transition and melt recrystallization mechanism.

On basis of the DSC data,  $X_{hc}$ ,  $X_{sc}$ , and  $f_{SC,DSC}$  of racemic blends were calculated, as illustrated in Figure 5. Because higher  $T_c$  facilitates the formation of more perfect and more ordered crystallites,  $X_{hc}$  increases with  $T_c$  at  $T_c < 140$  °C [Figure 5a (L144/D144)], which is consistent with the results of PLLA. Because SCs are more thermodynamically stable than their HC equivalents, high  $T_c$  is favorable for the formation of SCs. The  $X_{hc}$  of M-MW blends (L41/D41) and H-MW blends (L95/D95 and L144/D144) progressively decreases with  $T_c$  at  $T_c \geq 140$  °C and  $T_c \geq 160$  °C (Figure 5a), respectively. Their  $X_{sc}$  and  $f_{SC,DSC}$  (Figure 5b,c) suggested the favorable formation of SCs at high  $T_c$ . At  $T_c > 180$  °C, HCs completely disappear and SCs are exclusively formed. The reason is that the homocrystallization segments from the entangled chain remain amorphous at  $T_c > 180$  °C. As shown in Figure 4, the HC melting peak is below 180 °C. After the first heating up to 250 °C and cooling to 180 °C to keep crystallization, HCs kept the amorphous state, unable to form crystals.

The multicrystalline behavior of racemic blends shows an interesting MW dependence in the isothermal crystallization. At the same  $T_c$ ,  $X_{sc}$  decreases dramatically with increasing MWs (Figure 5b), demonstrating that the H-MW PLLA and PDLA are unfavorable for stereocomplexation. The L11/D11 blend has a large  $X_{sc}$  of 30–40%. The  $X_{sc}$  of M/H-MW racemic blends (L41/D41 and L144/D144) is less than 15% at all  $T_c$  values investigated, which is much smaller than the  $X_{hc}$  of racemic blends crystallized at  $T_c < 140$  °C. Tsuji et al. have reported that the racemic blends with UH-MWs hardly form SCs but only crystallize in HCs at  $T_c \leq 130$  °C.<sup>40</sup> Other groups and author think that the restrained stereocomplexation in H-MW racemic blends is ascribed to two aspects, namely low chain diffusion ability and restricted intermolecular crystal nucleation/growth.<sup>20</sup> These two aspects, i.e., the chain diffusion ability and intermolecular crystal nucleation/growth, are the core mechanism for the formation of stereocomplexes.

First, the chain diffusion is a crucial factor for stereocomplexation compared to homocrystallization due to the high level of mixing required between PLLA and PDLA chains in

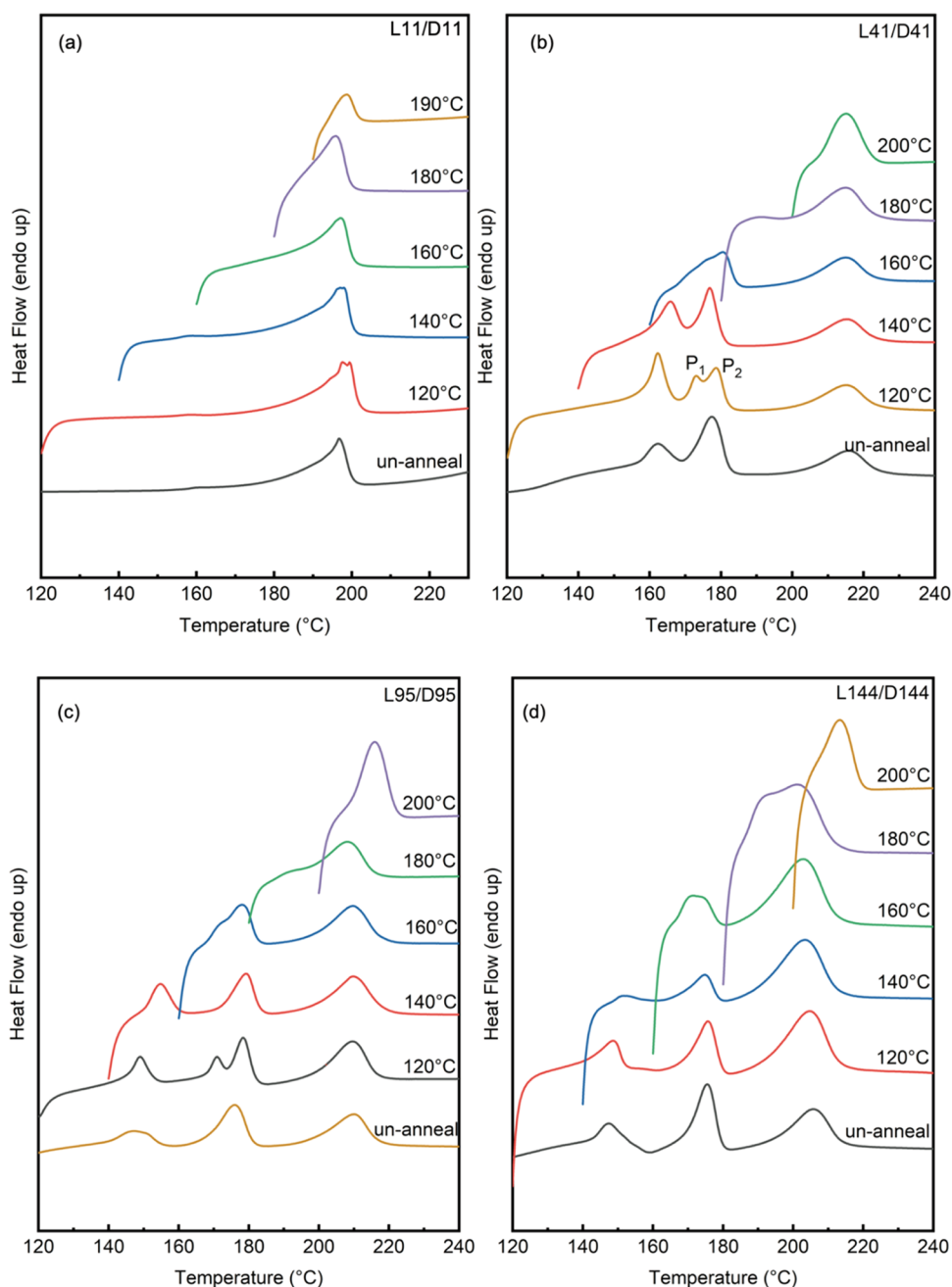


**Figure 4.** DSC melting curves of PLLA/PDLA racemic blends after isothermal melt crystallization at different temperatures: (a) L11/D11, (b) L41/D41, (c) L95/D95, and (d) L144/D144.

stereocomplexation. The chain length of the H-MW PLLA and PDLA has a higher viscosity and lower diffusion capacity compared to those of the L-MW PLA. In previous work, researchers have discovered that stereocomplexation precedes homocrystallization upon cooling the H-MW racemic blend.<sup>21</sup> Stereocomplexation between multiple chains will result in the formation of three-dimensional networks through physical crosslinks/entanglement. This can suppress the diffusion and mobility of bridging and surrounding chains. Furthermore, it has been well recognized that SCs can promote the heterogeneous nucleation of homocrystallization.<sup>18,45,46</sup> Thus, stereocomplexation suffers from a greater kinetic barrier than homocrystallization, even though it is more thermodynamically favorable.

Second, there are two external pathways for polymer crystal nucleation, namely intramolecular and intermolecular nuclea-

tions.<sup>47</sup> The former corresponds to folded-chain nucleation with most crystalline stems folded and truncated by the adjacent chain at the bundle-end surface, while the latter represents fringe spherule nucleation where all the crystalline stems extended out of the bundle-end surface. Because of the lower free energy barrier, the polymer may be willing to choose the pathway of intramolecular nucleation rather than intermolecular nucleation. Stereocomplexation between enantiomeric chains is a typical example of intermolecular crystal nucleation and growth. In the H-MW PLLA/PDLA racemic blends, intermolecular growth is more difficult than intramolecular growth, which may suppress stereocomplexation.<sup>21,23,48,49</sup> However, for the L-MW PLLA/PDLA racemic blends, the short chain length, high mobility, and intermolecular H-bond interactions between enantiomers may

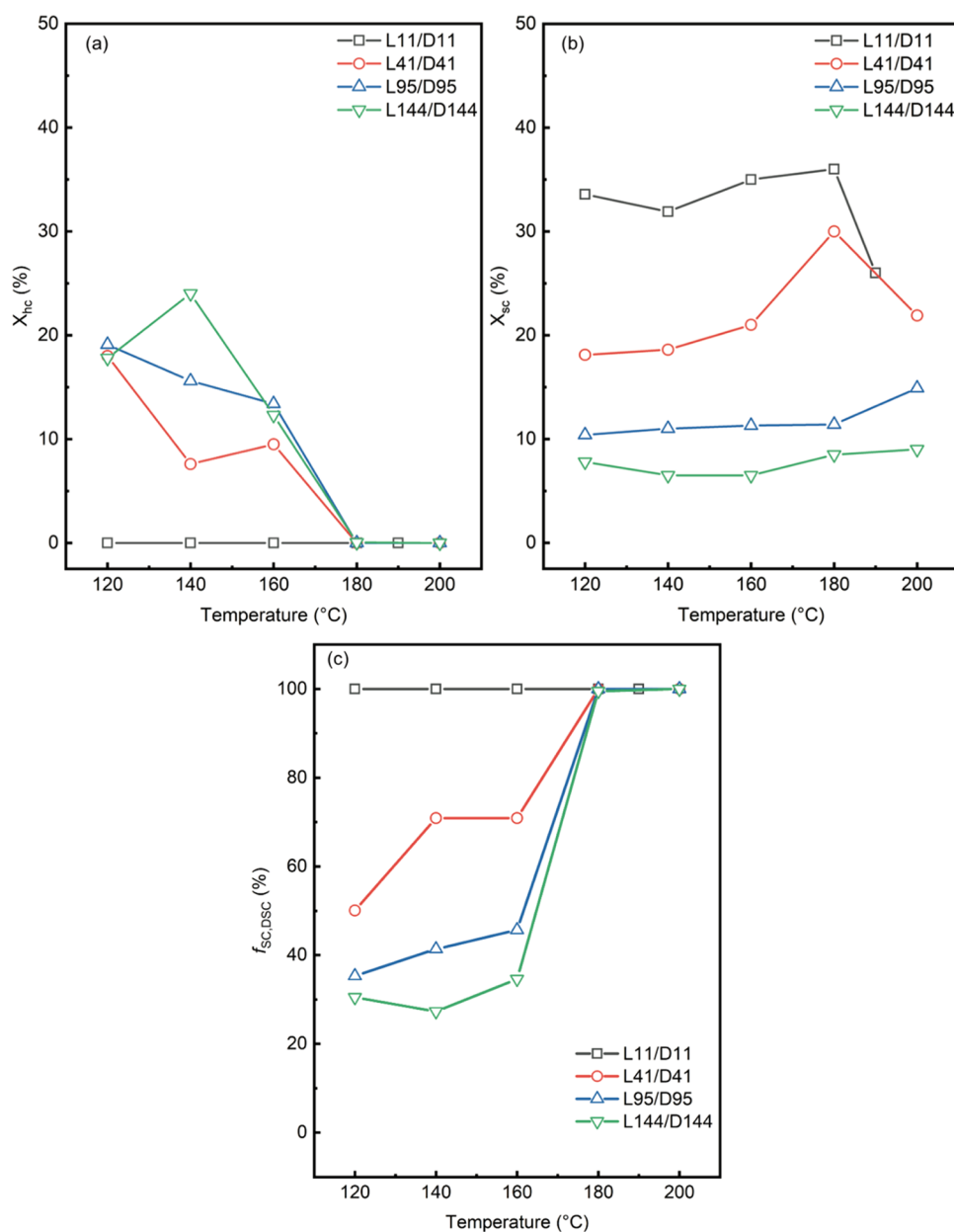


**Figure 5.** Degree of crystallinity of (a) HCs and (b) SCs and (c) relative fraction of SCs in symmetric PLLA/PDLA racemic blends after melt crystallization at different temperatures.

favor the intermolecular crystal nucleation and growth, resulting in the enhanced stereocomplexation.<sup>50</sup>

**4.3. Effects of the Molecular Weight and Mole Ratio for the Crystalline Structure of Asymmetric PLLA/PDLA Racemic Blends.** The crystal structure of the asymmetric PLLA/PDLA stereocomplexes was first well-established by assuming that the segmental length and the mole ratio of the two enantiomers are the same within a unit cell.<sup>51,52</sup> We thus first focused on the blends with the identical number of repeat units ( $x_L = x_D$ ) and equal amounts ( $n_L/n_D = 1:1$ ). In all the cases, a sharp endothermic melting peak was observed in each DSC thermograms (Figure 6a), which is about 50 °C higher than that of the HC of the parent PLLA or PDLA and in good agreement with the literature.<sup>53,54</sup> The melting temperature ( $T_m$ ) of the SCs decreases with increasing chain length (Figure 6a), contradicting/not following the correlation described by the Thomson–Gibbs equation (eq S1).<sup>55</sup> As the chain length

decreases, the enantiomeric chains would match each other in a more appropriate/suitable and uniform manner, which is determined by kinetic rather than thermodynamic factors. This difference is ascribed to the difference of stereocomplexes between irregular stereocomplexes or entanglement and the amorphous state and regular stereocomplexes. In other words, the melting temperature ( $T_m$ ) of the SC should increase as the chain length increases except for the imperfect crystallization of irregular stereocomplexes or entanglement and amorphous state.

Compared with the as-prepared samples, the crystallinity and degree of order significantly improve after an isothermal crystallization treatment (Figure S4). Apparently, there initially must be many defects within the crystals. With increasing  $T_c$ , the enantiomeric chains would match each other more appropriately dictated by thermodynamics rather than kinetic factors. We

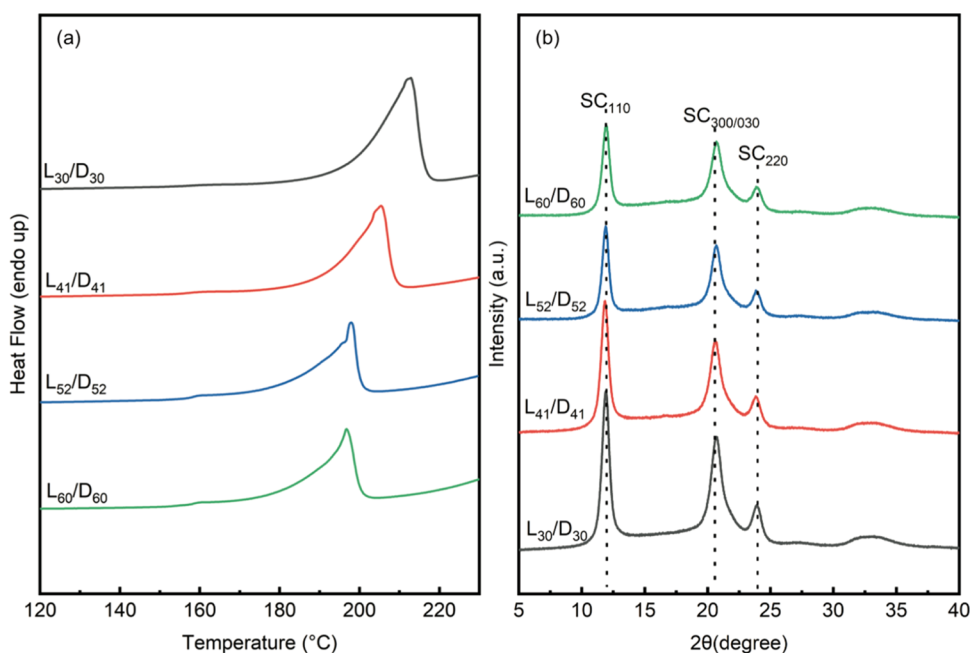


**Figure 6.** DSC thermograms (a) and XRD patterns (b) of SCs with equal mole ratios and the identical number of repeat units.

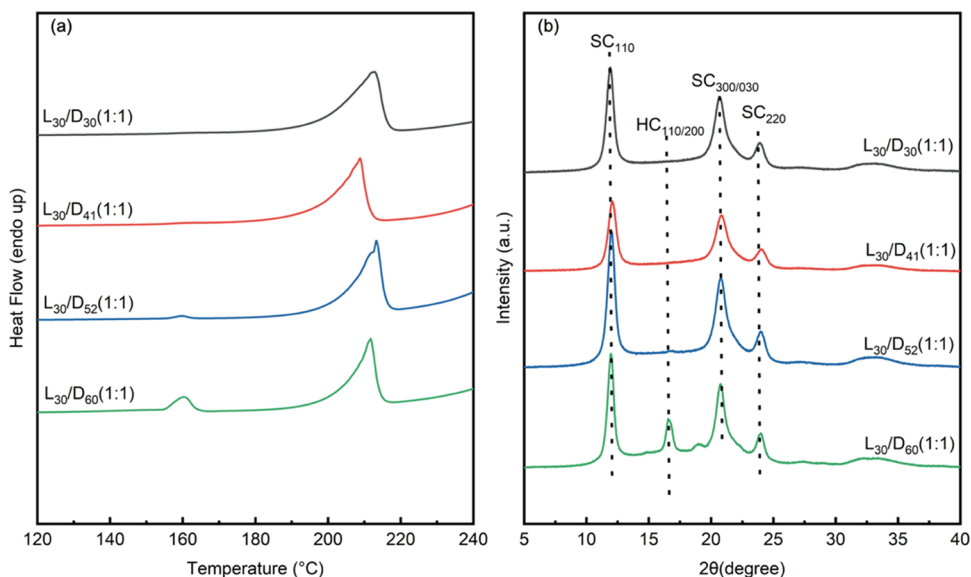


**Figure 7.** DSC thermograms (a) and XRD patterns (b) of  $L_{30}/D_y$  with equal mole ratios.

thus focus on a relatively higher temperature (120 °C) throughout POM images (Figure S9).

On the other hand, the formation of the SC is confirmed by three characteristic diffraction peaks at  $2\theta = 12.0$ ,  $21.0$ , and  $24.0^\circ$ , which correspond to the (110), (300)/(030), and (220) planes of the unit cells, respectively (Figure 6b).<sup>14,51,52</sup> Typical spherulitic morphologies were observed, with the diameter in the range of several hundred nanometers (Figure S9). The higher the crystallinity of SCs, the stronger the crystallization capacity and the faster the crystallization rate in the racemic blends. This is consistent with the phenomenon that the stereocomplexation precedes homocrystallization in isothermal crystallization of M/H-MW racemic blends.<sup>56</sup>

If the two enantiomeric chains are not of equivalent size, there will inevitably be redundant segments of the longer ones that cannot participate in the complexation. Several possible

scenarios can be envisaged: the overhanging segments could stay amorphous or can complex with another enantiomer (i.e., multicomplexation) or form HCs among themselves. These behaviors critically depend on the degree of chain length heterogeneity. To quantitatively reveal this effect, dissociated PLLA and PDLA with nonidentical dimensions ( $x_L \neq x_D$ ) but equal mole ratios ( $n_L/n_D = 1:1$ ) were mixed to form SCs.

Here, we take  $L_{30}/D_y$  (1:1) series as typical examples ( $y = 30, 41, 52, \text{ and } 60$ ). Distinct chain arrangements were observed with increasing  $y$ . When the difference of the chain length is not significant ( $y \leq 52$  represents  $x_L < x_D < 2x_L$ ), the blends form exclusively SCs, as confirmed by the characteristic diffractions in the XRD profile (Figure 7b). No sign of HCs was found. However, it does not indicate that there are no chain entanglements or amorphous states. Meanwhile, there is solely a single melting region (Figure 7a), ruling out the possibility of

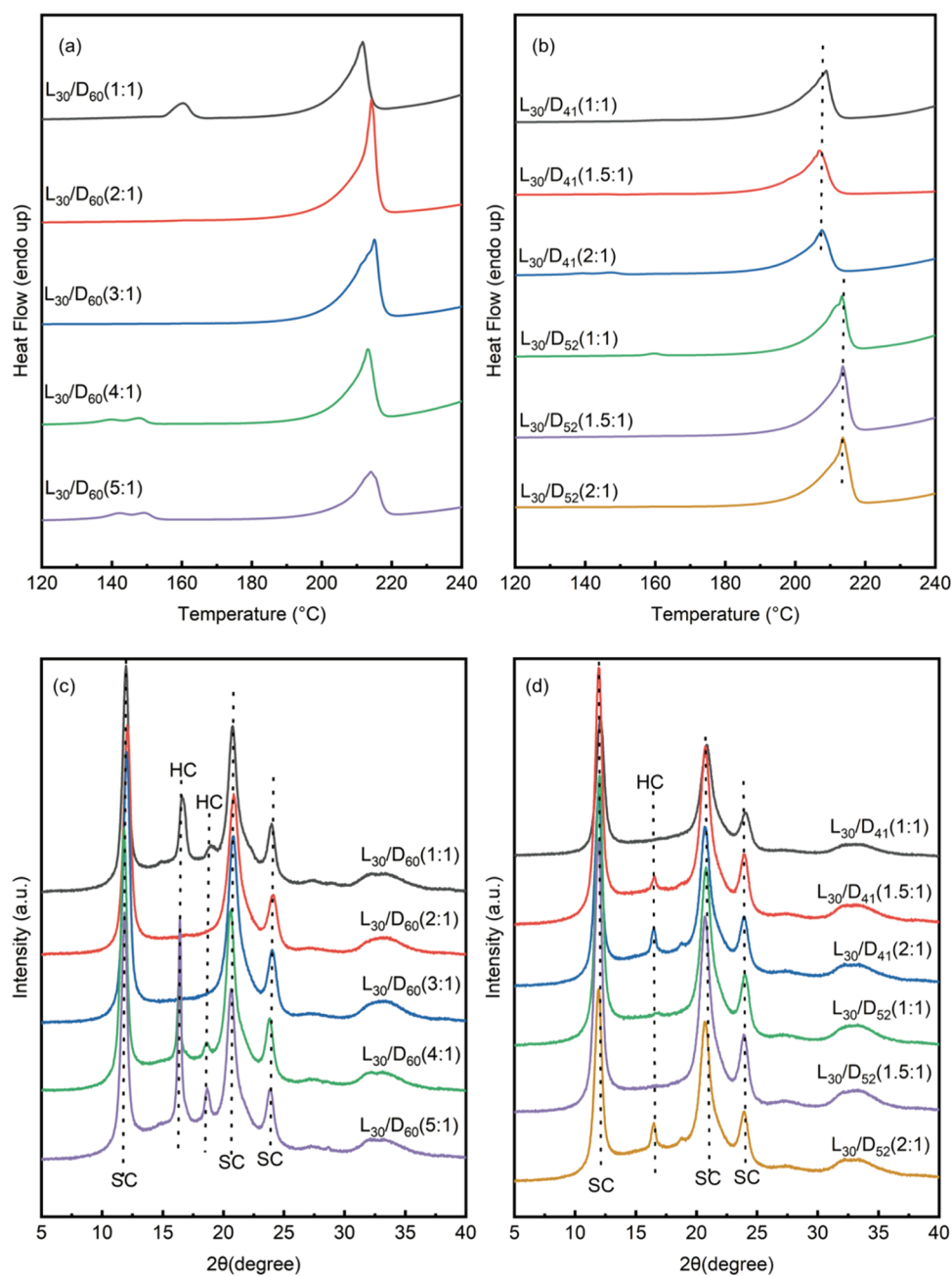


**Figure 8.** DSC thermograms of  $L_{30}/D_{60}$  (a) and  $L_{30}/D_n$  (b) and XRD patterns of  $L_{30}/D_{60}$  (c) and  $L_{30}/D_n$  (d) with different mole ratios.

multicomplexation. Since  $x_D$  is not longer than 2 times  $x_L$  ( $x_D < 2x_L$ ), a longer chain cannot accommodate two short chains in the series. Interestingly, without considering the different chain lengths ( $x_D$ ), the  $T_m$  of all these blends remains almost constant, close to that of  $L_{30}/D_{30}$  (1:1), demonstrating that all these SCs must have the same crystalline layer ( $d_c$ ) according to the Thomson–Gibbs equation (eq S1).<sup>55</sup> Thus, the thickness of the SC crystalline layer is limited by the length of the short chains, while the excess segments of the longer ones remain amorphous or contain crosslinks. We also parallelly studied a series of asymmetric PLLA/PDLA racemic blends with varying  $x_L$  and  $x_D$ , while keeping  $x_D < 2x_L$ . Similar behaviors are recorded in Figure S6. However, when the difference is significant ( $y = 60$  represents  $x_D \geq 2x_L$ ), the blends cannot form specifically uniform SCs, which has been confirmed by the characteristic diffractions in the XRD profile (Figure 8b). The sign of HCs was

found. Meanwhile, there were two melting peaks (Figure 8a), in which those around 160 and 211 °C belong to the HCs formed by the extra segments of PDLA<sub>60</sub> and the SC crystalline formed by asymmetric  $L_{30}/D_{60}$  (1:1) blends (Figure S5), respectively, and the result points sideways to the possibility of multicomplexation. The phenomenon will be discussed in more detail in the following sections.

Additionally, with further expansion of the chain length disparity ( $x_D \geq 2x_L$ ), there will be enough space in the longer chain to accommodate more than one short enantiomer, and multicomplexation becomes possible [e.g.,  $L_{30}/D_{60}$  (1:1)]. As straightforward evidence, the sample  $L_{30}/D_{60}$  (1:1) shows a rather different behavior compared to the above-mentioned cases [e.g.,  $L_{30}/D_{30}$  (1:1),  $L_{30}/D_{41}$  (1:1) and  $L_{30}/D_{52}$  (1:1)]. Under this circumstance, the second short chain could find enough room for complexation. Moreover, competitive

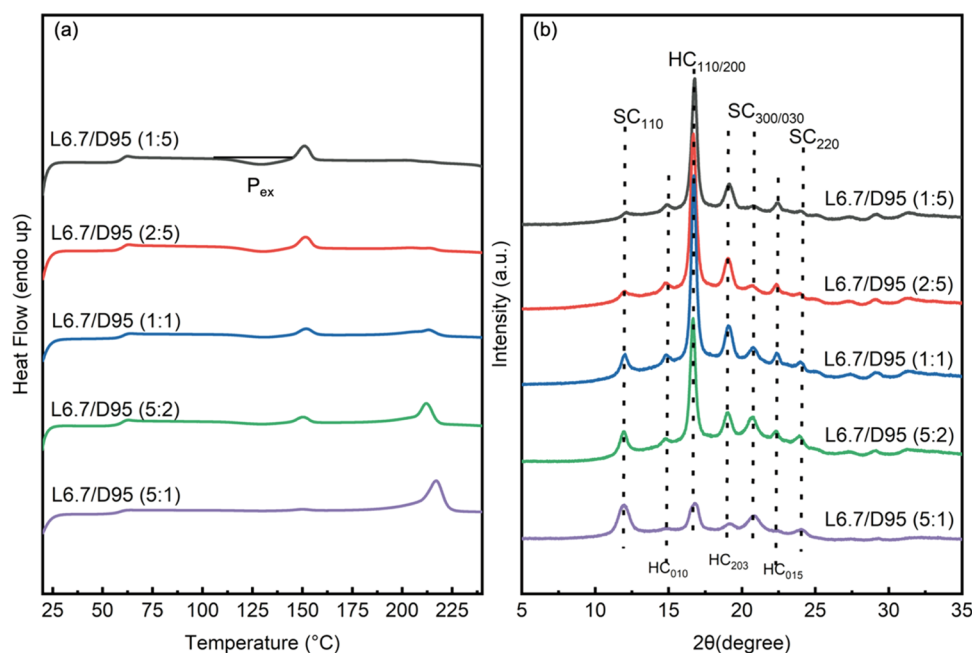


**Figure 9.** DSC thermograms (a) and XRD patterns (b) of L6.7/D95 with different mole ratios.

crystallization between SCs and HCs becomes nonnegligible, with the coexistence of SCs and HCs, as illustrated by the additional diffractions originating from HCs (Figures 7b and S5b).<sup>57</sup> In addition, two melting regions appear upon heating, the low- and high-temperature side endotherms are produced by the melting of homocrystals and stereocomplexes. All evidence indicates that segmental segregation occurred, with a portion of PDLA<sub>60</sub> forming independent HCs. In other words, HCs were formed among the redundant segments of the longer PLA chain. As a result, the molar ratios of the resultant SCs must deviate from the initial composition (i.e., 1:1).

The overhanging segments of PDLA<sub>60</sub> on the substrate surfaces of SCs could be further associated with an additional PLLA<sub>30</sub>. Due to chain folding, the formation of HCs would also become possible.<sup>47,50,58</sup> To further emphasize the mole ratio effect ( $n_L > n_D$ ), L<sub>30</sub>/D<sub>60</sub> with different compositions (2:1, 3:1, 4:1, and 5:1) were parallelly prepared, following the same protocol ( $x_D \geq 2x_L$ ). According to the above-mentioned argument, the optimal mole ratio for the L<sub>30</sub>/D<sub>60</sub> blends to form SCs is 2:1 and 3:1, while there will be excess PLLA<sub>30</sub> in the case of 3:1. In fact, compared with L<sub>30</sub>/D<sub>60</sub> (1:1), samples L<sub>30</sub>/D<sub>60</sub> (2:1) and L<sub>30</sub>/D<sub>60</sub> (3:1) form exclusively uniform SCs, while the formation of HCs fully disappeared (Figure 8a). Only the diffraction of the SC is identified by XRD (Figure 8c, red curve and blue curve). The melting peak of the PDLA<sub>60</sub> HC also disappears, leaving only an endothermal peak corresponding to the SC (Figure 8a). On the other hand, HCs reappear when the content of PLLA<sub>30</sub> was further increased. In the case of L<sub>30</sub>/D<sub>60</sub> (4:1) and L<sub>30</sub>/D<sub>60</sub> (5:1), HCs of excess PLLA<sub>30</sub> can be recognized in XRD (Figure 8c, green curve and purple curve) and DSC results (Figure 8a, green curve, and purple curve). The effects of the chain length on the formation of SCs in polymer blends have also been investigated computationally by other groups,<sup>28,59</sup> and the theoretical predictions are in good agreement with our experimental observations.

The analysis of the melting temperature provides deeper insights into the chain packing. A simplistic and direct inference would suggest that each PDLA<sub>60</sub> should associate with two

PLLA<sub>30</sub>. L<sub>30</sub>/D<sub>60</sub> (3:1) forms exclusively uniform SCs, which was confirmed by the characteristic diffractions in the XRD curves (Figure 8c). No sign of HCs was found. Meanwhile, there is only one single melting region (Figure 8a), excluding HCs of excess PLLA<sub>30</sub>. This is probably a result of the inability to form expanded chain conformations due to entanglement or HCs in the formation of less surplus PLLA<sub>30</sub> restrained by SCs in the formation of asymmetric L<sub>30</sub>/D<sub>60</sub>. For this reason, therefore, L<sub>30</sub>/D<sub>60</sub> (3:1) hardly forms SCs.

For further examining the assumption, PLLA and PDLA with nonidentical sizes ( $x_D < 2x_L$ ) and unequal mole ratios ( $n_L/n_D \neq 1:1$ ) were mixed to form SCs. L<sub>30</sub>/D<sub>41</sub>, L<sub>30</sub>/D<sub>52</sub>, L<sub>41</sub>/D<sub>52</sub>, and L<sub>52</sub>/D<sub>60</sub> with different compositions (1:1, 1.5:1, and 2:1) were parallelly prepared, following the same protocols ( $x_D < 2x_L$ ). As a result, we found that L<sub>30</sub>/D<sub>41</sub> (1.5:1 and 2:1) forms HCs, while L<sub>30</sub>/D<sub>52</sub> (1.5:1 and 2:1) cannot form HCs, as evidenced by the characteristic diffraction in the XRD curves (Figure 8d). Similar behaviors with L<sub>41</sub>/D<sub>52</sub> (1.5:1 and 2:1) and L<sub>52</sub>/D<sub>60</sub> (1.5:1 and 2:1) are recorded in Figure S6. In this situation that HCs the form of less surplus the short chain is restrained by SCs the form of asymmetric PLLA/PDLA blends is formation of SCs. As a result, homocrystallization takes place when there is a deviation from the equal molar ratio (Figures 8 and S5). The percentage of HCs increases as the amount of PLLA<sub>30</sub> increases (Figures 8a,c, and S5). In addition, the melting temperature ( $T_m$ ) difference between L<sub>30</sub>/D<sub>41</sub> and L<sub>30</sub>/D<sub>52</sub> is about 5 °C. This difference is ascribed to the difference in the thickness ( $d_c$ ) of stereocomplexes between L<sub>30</sub>/D<sub>41</sub> and L<sub>30</sub>/D<sub>52</sub>. The short chains (e.g., PLLA<sub>30</sub>) are unable to find an more appropriate and full path in SCs formed by PDLA<sub>41</sub>; this is not the case for PDLA<sub>52</sub>.

Based on what was mentioned above, it is reasonable to believe that the possibility of multicomplexation also exists in the M/H-MW PLLA/PDLA asymmetric blends. To investigate the possibility of multiple complexations in asymmetric M/H-MW PLLA/PDLA blends, the sample L6.7/D95 with different ratios (1:5, 2:5, 1:1, 5:2, 5:1) was prepared via solution blending for 3 days. As shown in Figure 9a, with the molar ratio of short chains (L6.7) increased, the melting peak of SCs increased and

the melting peak of HCs decreased, which was confirmed by the characteristic diffractions in the XRD curves (Figure 9b). Meanwhile, an exothermic phenomenon ( $P_{ex}$ ) prior to the melting region of HCs ( $\sim 150$  °C) corresponds to the transition from  $\alpha'$ -small to  $\alpha$ -large homocrystals.<sup>39,52,60,61</sup> Due to the  $\alpha'$ -to- $\alpha$  transition after heating, the melting point observed in the DSC curves of  $\alpha'$  crystals corresponds to the  $\alpha$  crystals formed in the phase transition.<sup>8</sup> It is worth noting that the HC melting region of L6.7/D95 (5:1) almost disappears (Figure 9a), but the HC diffraction still exists in Figure 9b. This is because a large number of SCs, which is not uniform because the entanglement is inevitable, inhibit the formation of HCs during the cooling crystallization process to maintain the amorphous state. Because the entanglement is unavoidable in L6.7/D95 (5:1), the short chains cannot be formed with closely packed SCs with the long chains. However, the existence of multicomplexation is undeniable.

In summary, we have mainly investigated the possibility of multicomplexation in asymmetric M/H-MW PLA blends with L-MW enantiomers. The problem of low-crystallinity SCs can be solved by multicomplexation, but the limitation of the method cannot be ignored. More importantly, high-crystallinity SCs are difficult to achieve in the processing of M/H-MW PLLA/PDLA blends.<sup>23</sup> Pan et al.<sup>20</sup> prepared the H-MW PLLA/PDLA (1:1) blends with various entanglement degrees by freeze drying, in which the entanglement density was tuned by varying the concentration of precursor polymer solutions. Disentangling facilitates the crystallization of SCs by not only accelerating the crystallization rate but also improving the SC crystallinity because the disentangled chains had higher diffusion ability, which favors the crystallization of SCs. Two aspects, namely, chain diffusion ability and intermolecular crystal nucleation/growth, are also the central mechanisms for the formation of stereocomplexes. Hence, these issues are the direction of our group as key factors to be addressed in the future.

## 5. CONCLUSIONS

The chain length and molar ratio effects cannot be neglected for the competitive mechanism of stereocomplexes (SCs) and homocrystals (HCs) in poly(lactic acid) (PLA) enantiomers. To systematically explore the critical contributions of both molecular weights and crystallization temperature and chain length and molar ratios to the formation of SCs, our group quantitatively prepared a wide MW range of symmetric and asymmetric PLA racemic blends, which contains L-MW PLLA with  $M_n > 6k$  g/mol. For investigating the  $T_c$  effect, we quantitatively prepared the symmetric PLLA/PDLA racemic blends to nonisothermal/isothermal melt crystallization at 120–180 °C. We observed that crystallinity and relative fraction of SCs increase with  $T_c$ , and the SCs are exclusively formed at  $T_c > 180$  °C in M/H-MW racemic blends. This can control the microstructure and physical performance of M/H-MW PLLA/PDLA blends. To investigate the MW effect, we quantitatively explored the critical contribution of chain length and mole ratios to the formation of SCs in L/M/H/UH-MW symmetric and L-MW asymmetric PLLA/PDLA blends. When MWs of one of the enantiomers are over 6k and less than 41k, the multiple stereocomplexation is clear in the asymmetric racemic blends. The resultant crystals adopt different molecular packing depending on the relative chain length. In general, when the two enantiomers have exactly the same chain length, more ordered SCs form with less entanglement or the amorphous region than for the MW of the enantiomers over 41k. On the other hand,

when the two components are not of equivalent size, the excess segments of the longer ones could stay amorphous on the basal surfaces or complex with other short enantiomers, depending on the difference in the chain length. Although there exists competitive crystallization between SCs and HCs, the former is preferred under an appropriate mole ratio; when the MW is over 41k and less than 200k, due to low chain diffusion ability and restricted intermolecular crystal nucleation/growth, SCs coexist with HCs. Based on this fact, to investigate the possibility of multiple complexations in asymmetric M/H-MW PLLA/PDLA blends, the problem of low-crystallinity SCs can be solved by multicomplexation. However, the limitation of the method cannot be ignored; when the MW exceeds 210k, the racemic blends are hardly/not able to form SCs. This study provides an insightful and comprehensive exploration into the stereocomplex crystallization mechanism of polymers and provides a reference value for future researchers attempting to prepare stereocomplex materials.

## ■ ASSOCIATED CONTENT

### Supporting Information

The Supporting Information is available free of charge at <https://pubs.acs.org/doi/10.1021/acsomega.2c05198>.

Experimental details and characterization data (PDF)

## ■ AUTHOR INFORMATION

### Corresponding Author

**Qinwei Gao** – College of Chemical Engineering, Nanjing Forestry University, Nanjing 210037, China; Co-Innovation Center of Efficient Processing and Utilization of Forest Resources, Nanjing Forestry University, Nanjing 210037, China; Email: [gqw@njfu.com.cn](mailto:gqw@njfu.com.cn)

### Authors

**Mingwei Guo** – College of Chemical Engineering, Nanjing Forestry University, Nanjing 210037, China; [orcid.org/0000-0002-0038-9904](https://orcid.org/0000-0002-0038-9904)

**Wenjing Wu** – College of Chemical Engineering, Nanjing Forestry University, Nanjing 210037, China

**Weixin Wu** – College of Chemical Engineering, Nanjing Forestry University, Nanjing 210037, China

Complete contact information is available at:

<https://pubs.acs.org/10.1021/acsomega.2c05198>

### Notes

The authors declare no competing financial interest.

## ■ ACKNOWLEDGMENTS

This work was supported by the National Natural Science Foundation of China (50573032, 31200451) and the Priority Academic Program Development of Jiangsu Higher Education Institutions (PAPD). The authors gratefully acknowledge the facilities support from Advanced Analysis and Testing Center of Nanjing Forestry University and Jiangsu Key Lab for the Chemistry & Utilization of Agricultural and Forest Biomass.

## ■ REFERENCES

(1) Aeschelmann, F.; Cams, M. Biobased Building Blocks and Polymers in the World: Capacities, Production, and Applications—Status Quo and Trends Towards 2020. *Ind. Biotechnol.* **2015**, *11*, 154–159.

- (2) Rasal, R. M.; Janorkar, A. V.; Hirt, D. E. Poly(lactic acid) modifications. *Prog. Polym. Sci.* **2010**, *35*, 338–356.
- (3) Raquez, J. M.; Habibi, Y.; Murariu, M.; Dubois, P. Polylactide (PLA)-based nanocomposites. *Prog. Polym. Sci.* **2013**, *38*, 1504–1542.
- (4) Prabakaran, M.; Grailer, J. J.; Pilla, S.; Steeber, D. A.; Gong, S. Amphiphilic Multi-Arm Block Copolymer Based on Hyperbranched Polyester, Poly(L-lactide) and Poly(ethylene glycol) as a Drug Delivery Carrier. *Macromol. Biosci.* **2009**, *9*, 515–524.
- (5) Yang, R.; Xu, G.; Dong, B.; Hou, H.; Wang, Q. A “Polymer to Polymer” Chemical Recycling of PLA Plastics by the “DE-RE Polymerization” Strategy. *Macromolecules* **2022**, *55*, 1726–1735.
- (6) Bai, H.; Deng, S.; Bai, D.; Zhang, Q.; Fu, Q. Recent Advances in Processing of Stereocomplex-Type Polylactide. *Macromol. Rapid Commun.* **2017**, *38*, No. 1700454.
- (7) Zhou, W.; Wang, K.; Wang, S.; Yuan, S.; Chen, W.; Konishi, T.; Miyoshi, T. Stoichiometry and Packing Structure of Poly(lactic acid) Stereocomplex as Revealed by Solid-State NMR and <sup>13</sup>C Isotope Labeling. *ACS Macro Lett.* **2018**, *7*, 667–671.
- (8) Pan, P.; Yang, J.; Shan, G.; Bao, Y.; Weng, Z.; Cao, A.; Yazawa, K.; Inoue, Y. Temperature-Variable FTIR and Solid-State <sup>13</sup>C NMR Investigations on Crystalline Structure and Molecular Dynamics of Polymorphic Poly(l-lactide) and Poly(l-lactide)/Poly(d-lactide) Stereocomplex. *Macromolecules* **2012**, *45*, 189–197.
- (9) Zhang, J.; Sato, H.; Tsuji, H.; Noda, I.; Ozaki, Y. Infrared Spectroscopic Study of CH<sub>3</sub>...OC Interaction during Poly(l-lactide)/Poly(d-lactide) Stereocomplex Formation. *Macromolecules* **2005**, *38*, 1822–1828.
- (10) Sarasua, J. R.; Rodríguez, N.; Arraiza, A.; Meaurio, E. Stereoselective Crystallization and Specific Interactions in Polylactides. *Macromolecules* **2005**, *38*, 8362–8371.
- (11) Feng, L.; Bian, X.; Li, G.; Chen, X. Compatibility and Thermal and Structural Properties of Poly(l-lactide)/Poly(l-co-d-lactide) Blends. *Macromolecules* **2022**, *55*, 1709–1718.
- (12) Feng, L.; Bian, X.; Li, G.; Chen, X. Thermal Properties and Structural Evolution of Poly(l-lactide)/Poly(d-lactide) Blends. *Macromolecules* **2021**, *54*, 10163–10176.
- (13) Baiardo, M.; Frisoni, G.; Scandola, M.; Rimelen, M.; Lips, D.; Ruffieux, K.; Wintermantel, E. Thermal and mechanical properties of plasticized poly(L-lactic acid). *J. Appl. Polym. Sci.* **2003**, *90*, 1731–1738.
- (14) Ikada, Y.; Jamshidi, K.; Tsuji, H.; Hyon, S. H. Stereocomplex formation between enantiomeric poly(lactides). *Macromolecules* **1987**, *20*, 904–906.
- (15) Tsuji, H.; Tezuka, Y. Stereocomplex Formation between Enantiomeric Poly(lactic acid)s. 12. Spherulite Growth of Low-Molecular-Weight Poly(lactic acid)s from the Melt. *Biomacromolecules* **2004**, *5*, 1181–1186.
- (16) Tsuji, H.; Takai, H.; Saha, S. K. Isothermal and non-isothermal crystallization behavior of poly(l-lactic acid): Effects of stereocomplex as nucleating agent. *Polymer* **2006**, *47*, 3826–3837.
- (17) Zhang, J.; Tashiro, K.; Tsuji, H.; Domb, A. J. Investigation of Phase Transitional Behavior of Poly(l-lactide)/Poly(d-lactide) Blend Used to Prepare the Highly-Oriented Stereocomplex. *Macromolecules* **2007**, *40*, 1049–1054.
- (18) Rahman, N.; Kawai, T.; Matsuba, G.; Nishida, K.; Kanaya, T.; Watanabe, H.; Okamoto, H.; Kato, M.; Usuki, A.; Matsuda, M.; Nakajima, K.; Honma, N. Effect of Polylactide Stereocomplex on the Crystallization Behavior of Poly(l-lactic acid). *Macromolecules* **2009**, *42*, 4739–4745.
- (19) Sun, Y.; He, C. Synthesis and Stereocomplex Crystallization of Poly(lactide)-Graphene Oxide Nanocomposites. *ACS Macro Lett.* **2012**, *1*, 709–713.
- (20) Sun, C.; Zheng, Y.; Xu, S.; Ni, L.; Li, X.; Shan, G.; Bao, Y.; Pan, P. Role of Chain Entanglements in the Stereocomplex Crystallization between Poly(lactic acid) Enantiomers. *ACS Macro Lett.* **2021**, *10*, 1023–1028.
- (21) Pan, P.; Han, L.; Bao, J.; Xie, Q.; Shan, G.; Bao, Y. Competitive Stereocomplexation, Homocrystallization, and Polymorphic Crystalline Transition in Poly(l-lactic acid)/Poly(d-lactic acid) Racemic Blends: Molecular Weight Effects. *J. Phys. Chem. B* **2015**, *119*, 6462–6470.
- (22) Tsuji, H. Poly(lactide) Stereocomplexes: Formation, Structure, Properties, Degradation, and Applications. *Macromol. Biosci.* **2007**, *7*, 1299.
- (23) Tsuji, H.; Ikada, Y. Stereocomplex formation between enantiomeric poly(lactic acids). 9. Stereocomplexation from the melt. *Macromolecules* **1993**, *26*, 6918–6926.
- (24) Tsuji, H.; Hyon, S. H.; Ikada, Y. Stereocomplex formation between enantiomeric poly(lactic acid)s. 3. Calorimetric studies on blend films cast from dilute solution. *Macromolecules* **1991**, *24*, 5651–5656.
- (25) Ren, J. M.; Lawrence, J.; Knight, A. S.; Abdilla, A.; Zerdan, R. B.; Levi, A. E.; Oschmann, B.; Gutekunst, W. R.; Lee, S.-H.; Li, Y.; McGrath, A. J.; Bates, C. M.; Qiao, G. G.; Hawker, C. J. Controlled Formation and Binding Selectivity of Discrete Oligo(methyl methacrylate) Stereocomplexes. *J. Am. Chem. Soc.* **2018**, *140*, 1945–1951.
- (26) Lamers, B. A. G.; van Genabeek, B.; Hennissen, J.; de Waal, B. F. M.; Palmans, A. R. A.; Meijer, E. W. Stereocomplexes of Discrete, Isotactic Lactic Acid Oligomers Conjugated with Oligodimethylsiloxanes. *Macromolecules* **2019**, *52*, 1200–1209.
- (27) Zhou, D.; Shao, J.; Sun, J.; Bian, X.; Xiang, S.; Li, G.; Chen, X. Effect of the different architectures and molecular weights on stereocomplex in enantiomeric poly(lactides)-b-MPEG block copolymers. *Polymer* **2017**, *123*, 49–54.
- (28) Xu, Y.; Wu, H.; Yang, J.; Liu, R.; Zhou, Z.; Hao, T.; Nie, Y. Molecular simulations of microscopic mechanism of the effects of chain length on stereocomplex formation in polymer blends. *Comput. Mater. Sci.* **2020**, *172*, No. 109297.
- (29) Zhou, D.; Xu, M.; Li, J.; Tan, R.; Ma, Z.; Dong, X.-H. Effect of Chain Length on Polymer Stereocomplexation: A Quantitative Study. *Macromolecules* **2021**, *54*, 4827–4833.
- (30) Purnama, P.; Kim, S. H. Stereocomplex Formation of High-Molecular-Weight Polylactide Using Supercritical Fluid. *Macromolecules* **2010**, *43*, 1137–1142.
- (31) Tashiro, K.; Wang, H.; Kouno, N.; Koshobu, J.; Watanabe, K. Confirmation of the X-ray-Analyzed Heterogeneous Distribution of the PDLA and PLLA Chain Stems in the Crystal Lattice of Poly(lactic acid) Stereocomplex on the Basis of the Vibrational Circular Dichroism IR Spectral Measurement. *Macromolecules* **2017**, *50*, 8066–8071.
- (32) Tashiro, K.; Kouno, N.; Wang, H.; Tsuji, H. Crystal Structure of Poly(lactic acid) Stereocomplex: Random Packing Model of PDLA and PLLA Chains As Studied by X-ray Diffraction Analysis. *Macromolecules* **2017**, *50*, 8048–8065.
- (33) Ye, G.; Wang, W.; Fan, D.; He, P. Effects of femtosecond laser micromachining on the surface and substrate properties of poly-lactic acid (PLA). *Appl. Surf. Sci.* **2021**, *538*, No. 148117.
- (34) Jia, S.; Yu, D.; Wang, Z.; Zhang, X.; Chen, L.; Fu, L. Morphologies, crystallization, and mechanical properties of PLA-based nanocomposites: Synergistic effects of PEG/HNTs. *J. Appl. Polym. Sci.* **2019**, *136*, 47385.
- (35) Pan, P.; Zhu, B.; Kai, W.; Dong, T.; Inoue, Y. Polymorphic Transition in Disordered Poly(l-lactide) Crystals Induced by Annealing at Elevated Temperatures. *Macromolecules* **2008**, *41*, 4296–4304.
- (36) Tsuji, H.; Bouapao, L. Stereocomplex formation between poly(L-lactic acid) and poly(D-lactic acid) with disproportionately low and high molecular weights from the melt. *Polym. Int.* **2012**, *61*, 442–450.
- (37) Di Lorenzo, M. L.; Androsch, R. Stability and Reorganization of  $\alpha'$ -Crystals in Random l/d-Lactide Copolymers. *Macromol. Chem. Phys.* **2016**, *217*, 1534–1538.
- (38) Uehara, H.; Karaki, Y.; Wada, S.; Yamanobe, T. Stereo-Complex Crystallization of Poly(lactic acid)s in Block-Copolymer Phase Separation. *ACS Appl. Mater. Interfaces* **2010**, *2*, 2707–2710.
- (39) Pan, P.; Kai, W.; Zhu, B.; Dong, T.; Inoue, Y. Polymorphic Crystallization and Multiple Melting Behavior of Poly(l-lactide): Molecular Weight Dependence. *Macromolecules* **2007**, *40*, 6898–6905.
- (40) Tsuji, H.; Sugimoto, S. Long terminal linear alkyl group as internal crystallization accelerating moiety of poly(l-lactide). *Polymer* **2014**, *55*, 4786–4798.

- (41) Avrami, M. Granulation, Phase Change, and Microstructure Kinetics of Phase Change. III. *J. Chem. Phys.* **1941**, *9*, 177–184.
- (42) Lorenzo, A. T.; Arnal, M. L.; Albuerno, J.; Müller, A. J. DSC isothermal polymer crystallization kinetics measurements and the use of the Avrami equation to fit the data: Guidelines to avoid common problems. *Polym. Test.* **2007**, *26*, 222–231.
- (43) Avrami, M. Kinetics of Phase Change. II Transformation-Time Relations for Random Distribution of Nuclei. *J. Chem. Phys.* **1940**, *8*, 212–224.
- (44) Vasanthan, N.; Ly, H.; Ghosh, S. Impact of Nanoclay on Isothermal Cold Crystallization Kinetics and Polymorphism of Poly(l-Lactic Acid) Nanocomposites. *J. Phys. Chem. B* **2011**, *115*, 9556–9563.
- (45) Schmidt, S. C.; Hillmyer, M. A. Polylactide stereocomplex crystallites as nucleating agents for isotactic polylactide. *J. Polym. Sci., Part B: Polym. Phys.* **2001**, *39*, 300–313.
- (46) Tsuji, H.; Takai, H.; Saha, S. K. Isothermal and non-isothermal crystallization behavior of poly(l-lactic acid): Effects of stereocomplex as nucleating agent: [Polymer 47 (2006) 3826-3837]. *Polymer* **2006**, *47*, 5430.
- (47) Wang, S.; Yuan, S.; Wang, K.; Chen, W.; Yamada, K.; Barkley, D.; Koga, T.; Hong, Y.-l.; Miyoshi, T. Intramolecular and Intermolecular Packing in Polymer Crystallization. *Macromolecules* **2019**, *52*, 4739–4748.
- (48) Woo, E. M.; Chang, L. Crystallization and morphology of stereocomplexes in nonequimolar mixtures of poly(l-lactic acid) with excess poly(d-lactic acid). *Polymer* **2011**, *52*, 6080–6089.
- (49) Chen, H.-P.; Nagarajan, S.; Woo, E. M. Unusual Radiating-Strip Morphology in Nonequimolar Mixtures of Poly(l-lactic acid) with Poly(d-lactic acid). *Macromolecules* **2020**, *53*, 2157–2168.
- (50) Chen, W.; Wang, S.; Zhang, W.; Ke, Y.; Hong, Y.-l.; Miyoshi, T. Molecular Structural Basis for Stereocomplex Formation of Polylactide Enantiomers in Dilute Solution. *ACS Macro Lett.* **2015**, *4*, 1264–1267.
- (51) Cartier, L.; Okihara, T.; Lotz, B. Triangular Polymer Single Crystals: Stereocomplexes, Twins, and Frustrated Structures. *Macromolecules* **1997**, *30*, 6313–6322.
- (52) Brizzolara, D.; Cantow, H.-J.; Diederichs, K.; Keller, E.; Domb, A. J. Mechanism of the Stereocomplex Formation between Enantiomeric Poly(lactide)s. *Macromolecules* **1996**, *29*, 191–197.
- (53) Wei, X.-F.; Bao, R.-Y.; Cao, Z.-Q.; Yang, W.; Xie, B.-H.; Yang, M.-B. Stereocomplex Crystallite Network in Asymmetric PLLA/PDLA Blends: Formation, Structure, and Confining Effect on the Crystallization Rate of Homocrystallites. *Macromolecules* **2014**, *47*, 1439–1448.
- (54) Shao, J.; Liu, Y.-l.; Xiang, S.; Bian, X.-c.; Sun, J.-r.; Li, G.; Chen, X.-s.; Hou, H.-q. The stereocomplex formation and phase separation of PLLA/PDLA blends with different optical purities and molecular weights. *Chin. J. Polym. Sci.* **2015**, *33*, 1713–1720.
- (55) Tan, R.; Zhou, D.; Liu, B.; Sun, Y.; Liu, X.; Ma, Z.; Kong, D.; He, J.; Zhang, Z.; Dong, X.-H. Precise modulation of molecular weight distribution for structural engineering. *Chem. Sci.* **2019**, *10*, 10698–10705.
- (56) Xie, Q.; Bao, J.; Shan, G.; Bao, Y.; Pan, P. Fractional Crystallization Kinetics and Formation of Metastable  $\beta$ -Form Homocrystals in Poly(l-lactic acid)/Poly(d-lactic acid) Racemic Blends Induced by Precedingly Formed Stereocomplexes. *Macromolecules* **2019**, *52*, 4655–4665.
- (57) Zhang, J.; Duan, Y.; Sato, H.; Tsuji, H.; Noda, I.; Yan, S.; Ozaki, Y. Crystal Modifications and Thermal Behavior of Poly(l-lactic acid) Revealed by Infrared Spectroscopy. *Macromolecules* **2005**, *38*, 8012–8021.
- (58) Jin, F.; Yuan, S.; Wang, S.; Zhang, Y.; Zheng, Y.; Hong, Y.-l.; Miyoshi, T. Polymer Chains Fold Prior to Crystallization. *ACS Macro Lett.* **2022**, *11*, 284–288.
- (59) Zhang, R.; Zha, L.; Hu, W. Intramolecular Crystal Nucleation Favored by Polymer Crystallization: Monte Carlo Simulation Evidence. *J. Phys. Chem. B* **2016**, *120*, 6754–6760.
- (60) Kawai, T.; Rahman, N.; Matsuba, G.; Nishida, K.; Kanaya, T.; Nakano, M.; Okamoto, H.; Kawada, J.; Usuki, A.; Honma, N.; Nakajima, K.; Matsuda, M. Crystallization and Melting Behavior of Poly(l-lactic Acid). *Macromolecules* **2007**, *40*, 9463–9469.
- (61) Zhang, J.; Tashiro, K.; Tsuji, H.; Domb, A. J. Disorder-to-Order Phase Transition and Multiple Melting Behavior of Poly(l-lactide) Investigated by Simultaneous Measurements of WAXD and DSC. *Macromolecules* **2008**, *41*, 1352–1357.